JACS
JOURNAL OF THE AMERICAN CHEMICAL SOCIETY

Communication

pubs.acs.org/JACS

Diameter-Specific Growth of Semiconducting SWNT Arrays Using Uniform Mo_2C Solid Catalyst

Shuchen Zhang, Lianming Tong, Yue Hu, Lixing Kang, and Jin Zhang*

Center for Nanochemistry, Beijing Science and Engineering Center for Nanocarbons, Beijing National Laboratory for Molecular Sciences, State Key Laboratory for Structural Chemistry of Unstable and Stable Species, College of Chemistry and Molecular Engineering, Peking University, Beijing 100871, P. R. China

Supporting Information

ABSTRACT: Semiconducting single-walled nanotube (s-SWNT) arrays with specific diameters are urgently demanded in the applications in nanoelectronic devices. Herein, we reported that by using uniform Mo_2C solid catalyst, aligned s-SWNT (~90%) arrays with narrow-diameter distribution (~85% between 1.0 and 1.3 nm) on quartz substrate can be obtained. Mo_2C nanoparticles with monodisperse sizes were prepared by using molybdenum oxide-based giant clusters, $(NH_4)_{42}[Mo_{132}O_{372}(H_3CCOO)_{30}(H_2O)_{72}]\cdot 10H_3CCOONH_4\cdot 300H_2O$($Mo_{132}$), as the precursor that was carburized by a gas mixture of C_2H_5OH/H_2 during a temperature-programmed reduction. In this approach, the formation of volatile MoO_3 was inhibited due to the annealing and reduction at a low temperature. As a result, uniform Mo_2C nanoparticles are formed, and their narrow size-dispersion strictly determines the diameter distribution of SWNTs. During the growth process, Mo_2C selectively catalyzes the scission of C−O bonds of ethanol molecules, and the resultant absorbed oxygen (O_{ads}) preferentially etches metallic SWNTs (m-SWNTs), leading to the high-yield of s-SWNTs. Raman spectroscopic analysis showed that most of the s-SWNTs can be identified as (14, 4), (13, 6), or (10, 9) tubes. Our findings open up the possibility of the chirality-controlled growth of aligned-SWNTs using uniform carbide nanoparticles as solid catalysts for practical nanoelectronics applications.

Nanoelectronic devices using single-walled carbon nanotubes (SWNTs) require pure semiconducting nanotubes with specific chirality.[1−3] However, the coexistence of metallic SWNTs (m-SWNTs) in as-grown samples dramatically lowers the performance of such devices, and sophisticated purification is usually necessary prior to device fabrication.[4−6] Furthermore, even for pure semiconducting SWNTs (s-SWNTs), the slight variation in diameter also leads to striking changes in their electronic properties.[7,8] These facts put forward the demanding challenge in the controlled growth of s-SWNT arrays with specific structure. To date, tremendous efforts have been devoted to selectively grow SWNTs of semiconducting type.[9,10] However, applicable approaches to effectively control their structures, that is, diameter and eventually chirality, are still lacking.

Generally, the diameter of SWNTs is directly defined by the size of the catalysts. Several attempts have been reported to control the diameter of catalysts to realize the narrow diameter distribution of SWNTs.[10−13] However, such routes still gave a relatively wide range of diameter of SWNTs due to the low melting point or nonuniform size of the catalysts. Recently, the cloning method has been developed to precisely control the diameter of as-grown SWNTs, but it still depends on the diameter of the nanotube seeds, and its efficiency is rather low.[14,15] In general, all these approaches to control the diameter of SWNTs are not capable of distinguishing s-SWNTs from metallic types, restricting their applications for nanoelectronic devices.

Solid catalysts have been shown extremely effective for the controlled growth of SWNTs due to that the crystalline structure can be retained during the growth process.[16] Among the solid catalysts, molybdenum-based nanoclusters have been widely used due to its highest melting point, above 2610 °C, among all the reported catalysts.[17] However, it is hard to obtain uniform Mo nanoparticles because of the formation of volatile MoO_3 during the annealing process of the precursors. However, Mo_2C is the most stable molybdenum carbide with a melting point of 2615 °C and can be easily transformed from Mo in the atmosphere of carbon. One of its unique catalytic capabilities is that the bare surface of Mo_2C is preferentially active for C−O cleavage of ethanol molecules to produce ethylene and absorbing oxygen (O_{ads}).[18] We have previously shown that the O_{ads} on the surface of catalysts can create an oxidizing environment to impede the growth of m-SWNTs.[19]

However, the difficulty to obtain Mo_2C nanoparticles of uniform sizes lies in the competitive formation of highly volatile MoO_3. In this work, we show that, by using a temperature-programmed reduction, the formation of MoO_3 can be greatly suppressed and that uniform Mo_2C nanoparticles can be obtained. Our TEM results confirmed that the nucleation of SWNTs was indeed on Mo_2C nanoparticles and the SWNTs grew along the (1 0 0) plane of Mo_2C. Combining its selective catalysis of C−O scission, we successfully obtained aligned s-SWNTs (~90%) arrays of narrow diameter-distribution (~85% between 1.0 and 1.3 nm) on a quartz substrate.

Figure 1a schematically illustrated the procedure of the approach. To obtain the uniform catalysts, $(NH_4)_{42}[Mo_{132}O_{372}(H_3CCOO)_{30}(H_2O)_{72}]\cdot 10H_3CCOONH_4\cdot$

Received: May 25, 2015
Published: July 10, 2015

DOI: 10.1021/jacs.5b05384
J. Am. Chem. Soc. 2015, 137, 8904−8907

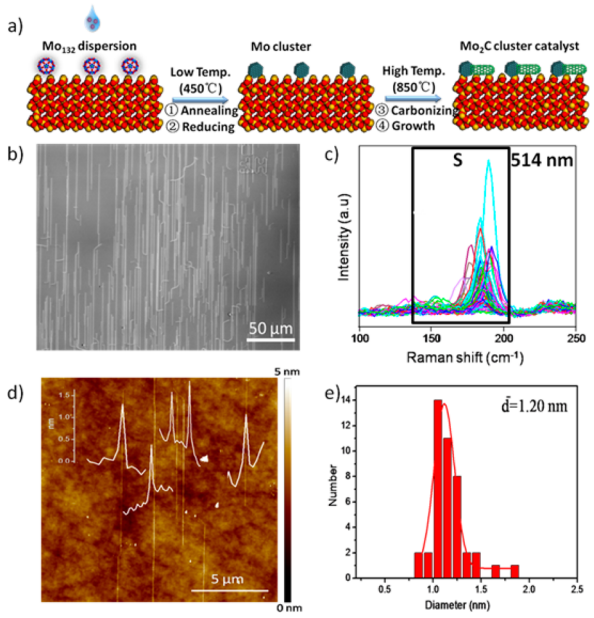

Figure 1. (a) Schematic illustration of the growth of horizontally aligned s-SWNT arrays using Mo_2C catalysts on a quartz substrate. (b) SEM image of Mo_2C catalyzed SWNT array. (c) Raman spectra in the RBM region of the nanotubes transferred to Si/SiO_2 (300 nm) substrate measured with 514 nm laser. A linear scan was performed over a distance of 200 μm with 1 μm step size. The black rectangle presents the RBM region where semiconducting (S) nanotubes can be detected using 514 nm laser. (d) AFM analysis of the as-grown SWNTs on substrate. The diameters of different nanotubes are almost identical. (e) The statistics of the diameters of the as-grown SWNTs. The average diameter is 1.20 nm with standard deviation 0.2 nm.

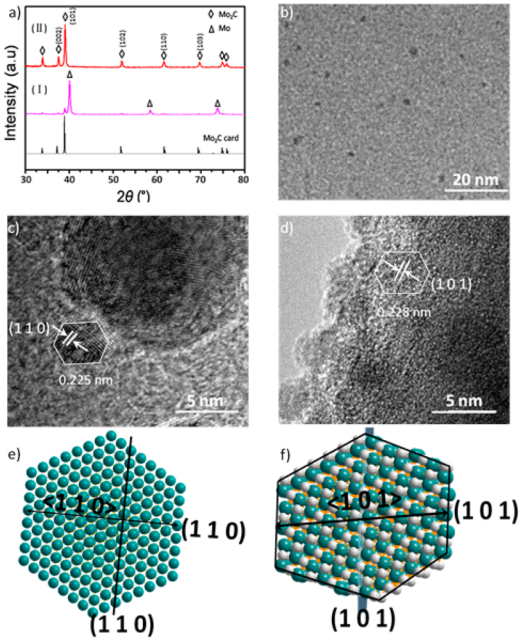

Figure 2. (a) XRD patterns of Mo_{132} after reducing (curve I) and reacting with ethanol (curve II), indicating the formation of Mo and Mo_2C, respectively. The black curve presents the standard Mo_2C card. (b) TEM image of the catalyst nanoparticles. (c,d) HRTEM images of Mo nanoparticle (c) and hexagonal Mo_2C nanoparticles (d). (e, f) Atomic models of Mo and Mo_2C nanoparticles, respectively (green, Mo; white, C).

$300H_2O$ (denoted as Mo_{132}) clusters were chosen as the catalyst precursor (for details see Experimental Section in Supporting Information). The Fourier transform infrared spectroscopy (IR), ultraviolet/visible (UV−vis) spectroscopy, and X-ray photoelectron spectroscopy (XPS) characterizations (shown in Figure S1) confirmed the structure of the clusters. As the size defined by its intrinsic structure of Mo_{132} is exactly the same for all the clusters, the sizes of the catalyst nanoparticles converted from it should in principle be the same. The Mo_{132} clusters were then spin-coated on a quartz substrate, annealed in air, and transferred to Mo_2C in carbon atmosphere. It is important to note that, in order to suppress the formation of MoO_3, a relatively low temperature, 300 °C, was necessary for the annealing and reduction. The formation of Mo_2C was clearly confirmed by X-ray diffraction (XRD) and high resolution TEM (HRTEM) shown in Figure 2, as well as XPS characterization shown in Figure S2. The diameter distribution of the Mo_2C nanoparticles was as narrow as 1.35 ± 0.2 nm (see Figure S3a ,c). For comparison, a wider diameter distribution (1.24 ± 0.4 nm, see Figure S3b,d) was observed if a higher temperature, 700 °C, was used. The SEM image of SWNT array grown using Mo_2C catalyst was given in Figure 1b, which shows well-aligned nanotubes at large scale of hundreds of microns.

In Figure 1c, Raman measurement of the radial breathing mode (RBM) with 514 nm excitation laser showed that most of the peaks are at ∼190 cm^{-1}, from which the SWNTs can be assigned as semiconducting tubes according to the Kataura-plot (k-plot). In addition, the corresponding tangential vibration (G mode) bands at ∼1580 cm^{-1} did not exhibit the Breit−Wigner−Fano (BWF) line shapes (see Figure S4), a typical feature of metallic SWNTs, further confirming the semiconducting characteristic of the nanotubes. In fact, the statistics of the RBM in the Raman spectra (both 514 and 633 nm excitation) gave an estimate of 95% of the s-SWNTs. The diameters of the SWNTs were directly measured from AFM measurements, see a typical image in Figure 1d. The statistics was given in Figure 1e. It is seen that 85% of the nanotubes are between 1.0 and 1.3 nm in diameter and that the diameter has a narrow distribution of 1.20 ± 0.2 nm. We note that the RMS of the quartz substrate is ±0.2 nm, so that the standard deviation of diameter distribution is in fact of the same value as the RMS of the substrate and could be overestimated. The diameter calculated from the RBM frequency according to the equation, $d = 248/\omega$ = 1.30 nm, also closely matches the average diameter measured by AFM. Strikingly, the SWNTs grown using 700 °C for annealing and reduction showed broader diameter distribution of 1.23 ± 0.4 nm (see Figure S5). The corresponding Raman spectra in Figure S6c,d showed a much broader distribution of the RBM frequencies, also indicating a much broader diameter distribution.

In order to confirm the formation of Mo_2C, we performed XRD and HRTEM characterization of the catalyst nanoparticles after the Mo_{132} clusters were reduced by H_2 and reacted with ethanol, respectively. After the temperature-programmed reduction by H_2, the XRD patterns of Mo were clearly observed, as shown by curve I (purple) in Figure 2a. The HRTEM image in Figure 2c showed a lattice fringe of 0.225 nm, corresponding to the crystal plane (1 0 0) of Mo, see the atomic model schemed in Figure 2e. During the growth procedure, the temperature was elevated to 850 °C and the ethanol was decomposed. The Mo nanoparticles were then converted to Mo_2C. A typical TEM image in Figure 2b showed the monodispersion of the nanoparticles. The formation of Mo_2C was evidenced by the XRD result shown by curve II (red) in Figure 2a, which presents

DOI: 10.1021/jacs.5b05384
J. Am. Chem. Soc. 2015, 137, 8904−8907

the exact same features as the standard Mo_2C card (black curve). The corresponding HRTEM image in Figure 2d showed the crystal plane of hexagonal Mo_2C (1 0 1) with lattice constant 0.228 nm (schemed in Figure 2f). XPS measurement in Figure S2 also indicated the formation of Mo−C bond.

Bulk hexagonal Mo_2C has a high melting point of ∼2615 °C and strong bonding between Mo and C, implying that the hexagonal Mo_2C nanoparticles should still be solid and maintain their crystalline structure with well-faceted shapes when heated to the growth temperature 850 °C.[16] To further correlate the crystalline structure of the Mo_2C nanoparticles and the chirality of the SWNTs, HRTEM was performed on a suspended SWNT grown directly on Si_3N_4 grids shown in Figure 3a. The inset

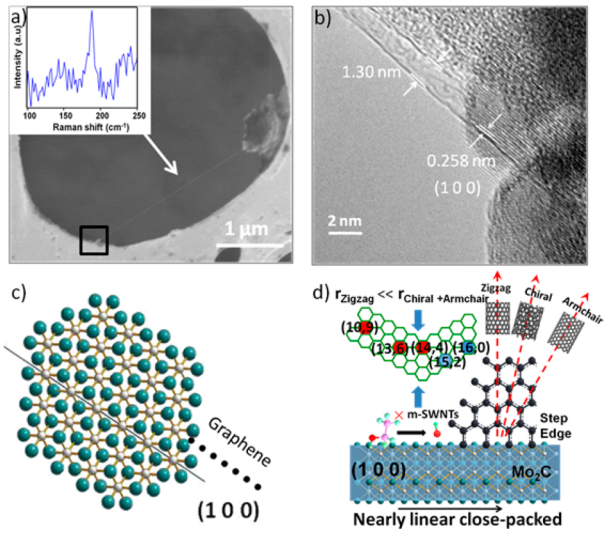

Figure 3. (a) TEM image of an individual suspended SWNT (indicated by the arrow). The inset shows the corresponding Raman spectra. (b) HRTEM image of the squared area in (a). The Mo_2C nanoparticle and the SWNT grown from it are clearly seen. (c) The side view of the (1 0 0) plane and a graphene sheet as an initial seed of SWNT. (d) The top view of the (1 0 0) plane to propose the correlation between the structures of the SWNTs and the Mo_2C nanoparticle. Metallic nanotubes are selectively etched due to the absorbing oxygen decomposed from ethanol molecules. The zigzag SWNTs, (16, 0) and (15, 2), are excluded due to the much slower kinetic growth rate. Only (14, 4), (13, 6), and (10, 9) nanotubes are obtained.

shows the distinct RBM peak at ∼190 cm^{-1}, from which the chirality can be assigned as (14, 4), (13, 6), or (10, 9) according to the k-plot. Figure 3b shows the magnified image of the squared area in Figure 3a, where the interface between a catalyst nanoparticle and a SWNT grown from it can be clearly seen. The diameter of the nanotube was 1.30 nm, in good agreement with the estimation from the position of the RBM peak (∼1.30 nm). The catalyst particle shows a lattice spacing of 0.258 nm corresponding to the (1 0 0) plane in hexagonal Mo_2C. Moreover, it is also obvious that the nanotube grows along the direction parallel to the (1 0 0) planes. To further understand the structure matching between the nanotube and catalyst nanoparticle, we propose the atomic models of the Mo_2C (1 0 0) plane and the initial graphene sheet in Figure 3c,d. Since the axis of the nanotube is parallel to the (1 0 0) planes, the initial graphene sheet should also grow parallel to the (1 0 0) planes, as schemed in Figure 3c. From the top view of the (1 0 0) plane in Figure 3d, it can be noticed that the Mo atoms align linearly at the top. It has been reported that the most stable structure exists only when the C−C bond is almost vertical to the bond between catalytic atoms.[20] This further confirms the parallel alignment of the graphene sheet to the (1 0 0) plane. Although the orientation of the graphene sheet is now determined, the direction of a SWNT's axis cannot be defined yet since the nanotube can grow along any direction in the (1 0 0) plane of Mo_2C (illustrated by the red arrows in Figure 3d). As discussed earlier, the m-SWNTs are inhibited due to the appearance of O_{ads} catalyzed by Mo_2C, thus only semiconducting nanotubes are possible. Further, the average diameter, 1.20 ± 0.2 nm, corresponds to five types of s-SWNTs, that is, (14, 4), (13, 6), (10, 9), (16, 0), or (15, 2). However, the kinetic growth rate of a zigzag tube is significantly (10−1000 times) slower than that of other CNTs,[21] so we can safely exclude the existence of zigzag and near-zigzag tubes, the (16, 0) or (15, 2) nanotubes, which is in good agreement with the Raman results as mentioned above. One should note that it is possible that one or two of the chiralities dominate in the as-grown s-SWNTs, which is difficult to distinguish in the present work. The chirality-selectivity is very sensitive to the temperature during growth. A change of ±50 °C results in much broader chirality distribution of the nanotubes, as shown in Figure S7.

Finally, to further evaluate the selectivity of s-SWNTs, electrical measurements of FETs fabricated on individual SWNTs were performed. Figure 4a,b shows the schematic

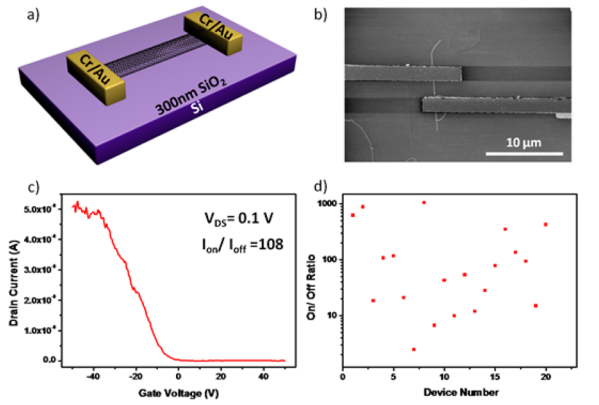

Figure 4. (a) Schematic illustration of an individual tube FET device. (b) SEM image of a FET device with a channel length of 2 μm. (c) Transfer characteristics of a semiconducting SWNT. An on/off ratio of 108 was observed. (d) The statistical result of I_{on}/I_{off} ratios from 20 randomly chosen nanotubes, indicating 90% of the nanotubes are semiconducting type.

illustration and SEM image of a typical FET device, respectively, fabricated on SWNTs transferred to a SiO_2/Si substrate with 300 nm SiO_2 dielectrics (for details see Experimental Section in Supporting Information). Highly doped Si was used as the back gate, and the source drain voltage was 0.1 V. The electron transfer characteristic of an s-SWNT is provided in Figure 4c. An on/off ratio of 108 was observed, indicating a typical semiconducting nanotube. The statistics of the on/off ratios of FET devices fabricated on 20 randomly chosen SWNTs is shown in Figure 4d. Two SWNTs with an on/off ratio lower than 10 were identified out of 20 randomly selected nanotubes. If the rule of thumb of on/off ratio 10 is applied to distinguish metallic and semiconducting nanotubes, the percentage of semiconducting tubes was estimated to be about 90%, consistent with the ratio obtained by Raman measurements.

In summary, uniform hexagonal Mo_2C solid catalyst, obtained from Mo_{132} as precursor, selectively catalyzes the scission of C−

DOI: 10.1021/jacs.5b05384
J. Am. Chem. Soc. 2015, 137, 8904−8907

O bond of ethanol, and the resultant O_{ads} preferentially etches metallic nanotubes. To inhibit the formation of MoO_3, the reducing reaction was conducted at a low temperature. As a result, we obtained s-SWNT arrays with narrow-diameter distribution (85% in 1.0−1.3 nm) with a density of 1 nanotube/5 μm on a quartz substrate. Furthermore, HRTEM characterization reveals that nanotubes grow parallel to the (1 0 0) planes of Mo_2C nanoparticles. The atomic models of Mo_2C and the initial graphene sheet at the early stage of the growth are proposed. Combined with our Raman measurements and the chirality assignment based on the k-plot, we finally assigned our s-SWNTs to three types, that is, (14, 4), (13, 6), or (10, 9). Finally, the FET devices using individual SWNTs were fabricated and the electronic transport measurement results reconfirmed that the selectivity of a s-SWNT array is as high as 90%. Our results paved the way toward practical applications of SWNTs with specific chirality in electronic devices. Nevertheless, the underlying mechanism of the chirality-selectivity is still to be further explored, and the controlled growth of s-SWNT arrays of single chirality and high density is still the ultimate goal to pursue for future electronic integrated circuits.

■ ASSOCIATED CONTENT

Supporting Information

Experimental details, detailed Raman spectrum analysis data, SEM images, HRTEM images, AFM images, and FET devices. The Supporting Information is available free of charge on the ACS Publications website at DOI: 10.1021/jacs.5b05384.

■ AUTHOR INFORMATION

Corresponding Author

*jinzhang@pku.edu.cn

Notes

The authors declare no competing financial interest.

■ ACKNOWLEDGMENTS

This work was supported by NSFC (21233001, 21129001, 51272006, 51432002, and 51121091) and MOST (2011CB932601).

■ REFERENCES

(1) Franklin, A. D. *Nature* **2013**, *498*, 443.
(2) Shulaker, M. M.; Hills, G.; Patil, N.; Wei, H.; Chen, H. Y.; PhilipWong, H. S.; Mitra, S. *Nature* **2013**, *501*, 526.
(3) Hu, Y.; Kang, L. X.; Zhao, Q. C.; Zhong, H.; Zhang, S. C.; Yang, L. W.; Wang, Z. Q.; Lin, J. J.; Li, Q. W.; Zhang, Z. Y.; Peng, L. M.; Liu, Z. F.; Zhang, J. *Nat. Commun.* **2015**, *6*, 6099.
(4) Hong, G.; Zhou, M.; Zhang, R. O. X.; Hou, S. M.; Choi, W.; Woo, Y. S.; Choi, J. Y.; Liu, Z. F.; Zhang, J. *Angew. Chem., Int. Ed.* **2011**, *50*, 6819.
(5) Cao, Q.; Han, S. J.; Tulevski, G. S. *Nat. Commun.* **2014**, *5*, 5071.
(6) Cao, Q.; Han, S. J.; Tulevski, G. S.; Zhu, Y.; Lu, D. D.; Haensch, W. *Nat. Nanotechnol.* **2013**, *8*, 180.
(7) Liu, Q. F.; Ren, W. C.; Chen, Z. G.; Wang, D. W.; Liu, B. L.; Yu, B.; Li, F.; Cong, H. T.; Cheng, H. M. *ACS Nano* **2008**, *2*, 1722.
(8) Zhou, W. W.; Zhan, S. T.; Ding, L.; Liu, J. *J. Am. Chem. Soc.* **2012**, *134*, 14019.
(9) Hong, G.; Zhang, B.; Peng, B. H.; Zhang, J.; Choi, W. M.; Choi, J. Y.; Kim, J. M.; Liu, Z. F. *J. Am. Chem. Soc.* **2009**, *131*, 14642.
(10) Kang, L. X.; Hu, Y.; Liu, L. L.; Wu, J. X.; Zhang, S. C.; Zhao, Q. C.; Ding, F.; Li, Q. W.; Zhang, J. *Nano Lett.* **2015**, *15*, 403.
(11) Cheung, C. L.; Kurtz, A.; Park, H.; Lieber, C. M. *J. Phys. Chem. B* **2002**, *106*, 2429.
(12) Li, Y. M.; Kim, W.; Zhang, Y. G.; Rolandi, M.; Wang, D. W.; Dai, H. J. *J. Phys. Chem. B* **2001**, *105*, 11424.
(13) Chen, Y.; Zhang, J. *Carbon* **2011**, *49*, 3316.
(14) Yao, Y.; Feng, C.; Zhang, J.; Liu, Z. *Nano Lett.* **2009**, *9*, 1673.
(15) Liu, J.; Wang, C.; Tu, X. M.; Liu, B. L.; Chen, L.; Zheng, M.; Zhou, C. W. *Nat. Commun.* **2012**, *3*, 1199.
(16) Yang, F.; Wang, X.; Zhang, D.; Yang, J.; Luo, D.; Xu, Z.; Wei, J.; Wang, J.-Q.; Xu, Z.; Peng, F.; Li, X.; Li, R.; Li, Y.; Li, M.; Bai, X.; Ding, F.; Li, Y. *Nature* **2014**, *510*, 522.
(17) An, L.; Owens, J. M.; McNeil, L. E.; Liu, J. *J. Am. Chem. Soc.* **2002**, *124*, 13688.
(18) Kelly, T. G.; Chen, J. G. *Green Chem.* **2014**, *16*, 777.
(19) Zhang, S. C.; Hu, Y.; Wu, J. X.; Liu, D.; Kang, L. X.; Zhao, Q. C.; Zhang, J. *J. Am. Chem. Soc.* **2015**, *137*, 1012.
(20) Zhu, H.; Suenaga, K.; Wei, J.; Wang, K.; Wu, D. J. *J. Cryst. Growth* **2008**, *310*, 5473.
(21) Yuan, Q.; Ding, F. *Angew. Chem., Int. Ed.* **2015**, *54*, 5924.

DOI: 10.1021/jacs.5b05384
J. Am. Chem. Soc. 2015, 137, 8904−8907